Progress in Nuclear Energy 99 (2017) 38–48

Contents lists available at ScienceDirect

Progress in Nuclear Energy

journal homepage: www.elsevier.com/locate/pnucene

Ruthenium transport in an RCS with airborne CsI

Teemu Kärkelä [a, *], Ivan Kajan [b], Unto Tapper [a], Ari Auvinen [a], Christian Ekberg [b]

[a] VTT Technical Research Centre of Finland Ltd, FI-02044 Espoo, Finland
[b] Chalmers University of Technology, SE-41296 Göteborg, Sweden

ARTICLE INFO

Article history:
Received 11 July 2016
Received in revised form
18 April 2017
Accepted 19 April 2017
Available online 5 May 2017

Keywords:
Ruthenium
Caesium iodide
Aerosol
Severe accident
Source term

ABSTRACT

Ruthenium is one of the most radiotoxic fission products which can be released from fuel as ruthenium oxides in an air ingress accident at a nuclear power plant. In this study it was found that the transport of the released ruthenium oxides through a reactor coolant system into the containment building is significantly affected by the atmospheric conditions. Airborne CsI increased the transport of gaseous ruthenium compared with that in a pure air atmosphere. The overall transport of ruthenium increased with temperature. In order to understand the behaviour of ruthenium in accident conditions, it is important to widen the experimental conditions from pure air/steam atmospheres to more realistic mixtures of prototypic gases and aerosols.

1. Introduction

During normal operation of a nuclear power plant (NPP), fission products are produced in the fuel pellets, e.g. UO_2, as by-products of a neutron radiation-stimulated fission reaction. The produced fission products are retained within the fuel matrix and in a gas space between the cladding material and fuel pellet. In a severe nuclear power plant accident, when coolant is lost from the reactor and the reactor temperature increases, degradation of fuel pellets takes place eventually. As the integrity of fuel pellet cladding material is lost, release of fission products from the pellets is initiated and if the source term mitigation measures are insufficient, radiotoxic compounds may be transported into the environment. This causes a threat to the population, particularly to the employees of the NPP, as radiation may cause diseases, such as cancer, when citizens are exposed to fission products via deposition on the skin or when airborne fission products are inhaled and ingested or when the radiation dose rate in the environment is significantly increased.

Release of the fission product ruthenium from nuclear fuel occurs when the metallic ruthenium is oxidized to gaseous RuO_2, RuO_3 and RuO_4. When the temperature decreases below approx. 1000 K, the released RuO_2 has already condensed to solid RuO_2, whereas RuO_3 has decomposed to RuO_2 and then also condensed to solid RuO_2. Therefore, only RuO_4 can be observed in gaseous form at low temperatures. The impact of oxidizing conditions on ruthenium release and transport has been studied previously. The main emphasis has been on ruthenium chemistry in pure air and steam/air atmospheres. In large-scale Phébus FP experiments (Haste et al., 2013; Grégoire and Haste, 2013) it was observed that most of the released ruthenium was transported to the containment building as solid RuO_2. Small-scale experiments (Backman et al., 2005; Kärkelä et al., 2007; Vér et al., 2012) have shown that the transport of gaseous ruthenium through a reactor coolant system (RCS) into the containment building can be much higher than would be expected on the basis of thermodynamic equilibrium calculations. It was observed that the decomposition of gaseous RuO_4 was not complete and it did not follow the equilibrium model when the residence time of gas flow was short in the high temperature gradient area of a model primary circuit (Kärkelä et al., 2014). As a result, the observed partial pressure of RuO_4 in containment conditions was at a level of 10^{-6} to 10^{-8} bar at 310 K–400 K. The research on air ingress conditions was taken even further in a recent study (Kajan et al., 2017a), in which the air radiolysis products N_2O, NO_2 and HNO_3 with representative concentrations were fed into the flow of ruthenium oxides in a model primary circuit. Both NO_2 and HNO_3 appeared to be efficient in oxidizing lower ruthenium oxides to RuO_4 and increasing the transport of gaseous ruthenium beyond the previous observations in pure air and steam/air atmospheres.

In addition to gaseous additives, the gas flow in a reactor coolant

* Corresponding author.
E-mail address: teemu.karkela@vtt.fi (T. Kärkelä).

http://dx.doi.org/10.1016/j.pnucene.2017.04.019

Abbreviations

AS	aspiration sampler
CMD	count median diameter
CO	critical orifice
CPC	condensation particle counter
DMA	differential mobility analyzer
ELPI	electrical low pressure impactor
HPGe	high purity germanium detector
ICP-MS	inductively coupled plasma mass spectrometry
INAA	instrumental neutron activation analysis
MFC	mass flow controller
NPP	nuclear power plant
PTFE	polytetrafluoroethylene
RCS	reactor coolant system
SEM	scanning electron microscope
SMPS	scanning mobility particle sizer
T/P	temperature and pressure
XPS	X-ray photoelectron spectroscopy
ρ_0	reference density (1 g/cm3)
ρ_p	particle density
C_s (d_a)	Cunningham slip correction factor for the aerodynamic diameter
C_s (d_m)	Cunningham slip correction factor for the mobility diameter
C_s (d_ve)	Cunningham slip correction factor for the volume equivalent diameter
d_a	aerodynamic diameter
d_m	(electrical) mobility diameter
d_ve	volume equivalent diameter
χ	dynamic shape factor

system in severe accident conditions also includes aerosols, formed by fission products and control rod materials. The effect of aerosols on the transport and speciation of ruthenium has not been studied extensively. In a previous study with silver particles fed into the flow of ruthenium oxides (Kajan et al., 2017b), the transport of gaseous ruthenium decreased significantly as RuO_4 condensed to RuO_2 on the surface of silver particles. Another representative compound in the primary circuit is radiotoxic caesium iodide, which is the most important form of iodine transported into the containment atmosphere (Clément et al., 2007). There is some evidence of the retention of ruthenium on a surface coated with caesium at high temperature (750–900 K) (Vér et al., 2010) and of the trapping of gaseous ruthenium by CsI deposit at low temperature (ca. 300 K) (Kärkelä et al., 2007). However, the effect of airborne CsI on the transport of ruthenium in an RCS is not known. The aim of this study was to focus on the behaviour of Ru-CsI system in the gas phase and to determine experimentally whether CsI would be able to affect the ruthenium transport through an RCS in air ingress conditions.

2. Experimental

2.1. Experimental facility

The configuration of the "VTT Ru transport facility" used in these experiments is presented in Fig. 1. A detailed description of the facility was presented in the previous studies (Kärkelä et al., 2007; Kajan et al., 2017a). The main component of the facility was the horizontal, tubular flow furnace (Entech, ETF20/18-II-L), which was used to heat the anhydrous RuO_2 powder (99.95%, Alfa Aesar). The furnace was 110 cm long and it had two heating sections, each 40 cm long. These zones were separated by a 38 mm layer of insulation. At both ends of the furnace there was a 131 mm thermal insulation. The furnace tube was made of high purity alumina (Al_2O_3, 99.7%) and its inner diameter was 22 mm. The alumina crucible with the RuO_2 powder (mass ca. 1 g) was placed in the middle of the second heated zone of the furnace. The RuO_2 powder was heated to 1300 K, 1500 K or 1700 K in an oxidizing flow in order to produce gaseous ruthenium oxides.

The total air flow rate through the facility was 5.0 ± 0.1 l/min (NTP; NTP conditions 0 °C, 101325 Pa, measured with a Thermal Mass Flowmeter TSI 3063, TSI Incorp.). The pressure inside the facility ranged from 102 to 104 kPa. The air flow directed to the furnace tube was either dry or humid. In the case of dry atmosphere, the air flow of 5.0 ± 0.1 l/min (NTP) was directed to the furnace. In the case of humid atmosphere, the air flow 2.50 ± 0.05 l/min (NTP) was fed through an atomizer (TSI 3076) and the flow transported the droplets (Milli-Q, ultrapure water, resistivity 18.2 MΩ cm at 25 °C) produced by the atomizer via the heated line (120 °C) to the furnace. The gas flow was mixed with another air flow 2.50 ± 0.05 l/min (NTP) before the inlet of furnace. Water evaporated when the droplets were heated, thus it led to an increase in the steam concentration within the furnace. CsI (99.999%, Sigma-Aldrich) was fed to the facility by mixing CsI powder with ultrapure water in the supply bottle of the atomizer and the generated droplets transported CsI to the furnace tube. As water evaporated from the droplets, the formation of solid CsI particles occurred.

After the vaporization of Ru and the subsequent reactions within the gaseous atmosphere, the gaseous and particulate reaction products were trapped in NaOH solution and collected on plane polytetrafluoroethylene (PTFE) filter (see "filter 1" in Fig. 1), respectively, at the outlet of the facility where temperature had decreased to ca. 300 K. Particle samples were also collected on perforated carbon-coated nickel (400 mesh) grids with the aspiration sampler. An additional PTFE filter (see "filter 2" in Fig. 1) was placed into the aerosol online analysis line to enable particle chemical analysis after the experiment, see below. A detailed description of the facility is given in (Kajan et al., 2017b). The details of particle online analysis are given below.

2.2. Experimental procedure and matrix

The experiments were started with placing a crucible filled with RuO_2 powder (1 g) into the furnace and then heating up the system (heating rate of 10 °C per minute). A nitrogen gas flow of 0.50 ± 0.01 l/min (NTP) was directed through the facility during the heating up phase in order to flush out the oxygen in the system. The main gas flow through the facility was started when the furnace set-point was reached. In the experiments, particulate and gaseous reaction products were collected on filter and trapped in a 1 M NaOH solution, respectively. At the same time, particles in the gas phase were analysed online and additional samples of the particles were collected for the analyses to be conducted later. After the experiment, the gas flows were stopped and the filters and trapping solutions were removed. The facility was sealed airtight. When the facility was cooled down after several hours (cooling rate of 10 °C per minute), the crucible was removed.

The experimental matrix is presented in Table 1. Experiments 1 to 3 were conducted in pure dry or humid air atmosphere without aerosol additives. These experiments are also considered as reference experiments for experiments 4 to 6, which were conducted in

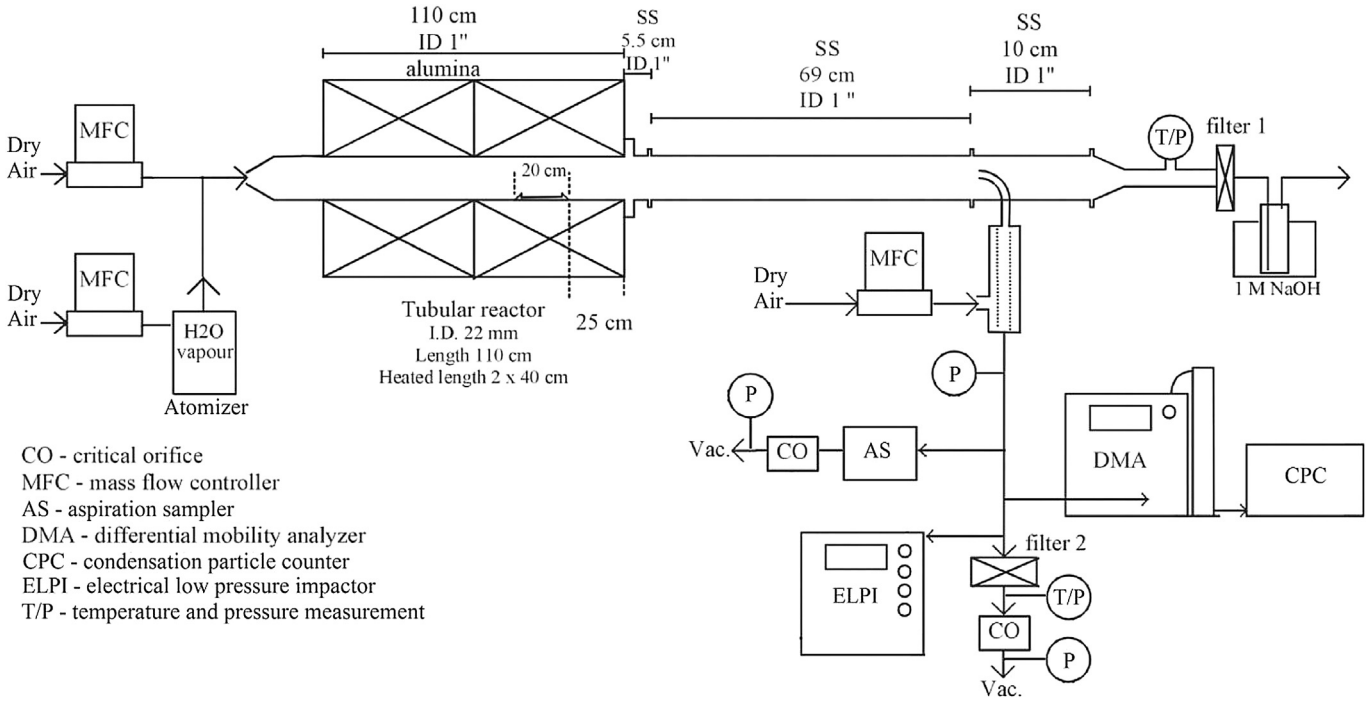

Fig. 1. Schematics of the experimental facility for ruthenium transport studies.

Table 1
The experimental matrix.

Exp	T [K]	Gas[a]	Precursor	Additive precursor conc.	Humidity[b] [ppmV]	Duration [min]
1 [ref. (Kärkelä et al., 2007)]	1300 ± 12	Air	1 g RuO_2	–	dry	45
2	1500 ± 12	Air	1 g RuO_2	–	2.1E4±2.1E3	51
3 [ref. (Backman et al., 2005)]	1700 ± 12	Air	1 g RuO_2	–	dry	20
4 CsI	1300 ± 12	Air	1 g RuO_2	CsI 4 wt %	2.1E4±2.1E3	30
5 CsI	1500 ± 12	Air	1 g RuO_2	CsI 4 wt %	2.1E4±2.1E3	30
6 CsI	1700 ± 12	Air	1 g RuO_2	CsI 4 wt %	2.1E4±2.1E3	30

[a] Total air flow rate through the furnace over the crucible was 5.0 ± 0.1 l/min (NTP) in every experiment.
[b] Humidity in the gas flow originated from the water-based precursor solution of the atomizer.

humid air atmosphere with CsI aerosol additive. Experiments 1 and 3 were performed in the previous studies (Kärkelä et al., 2007) and (Backman et al., 2005), respectively, with the same facility as in this study. The duration of experiments was from 20 to 51 min for the experiments without additives and 30 min for the experiments with CsI additive.

2.3. Online analysis of particles

The number size distribution of particles was measured online with a combination of a differential mobility analyzer (DMA, TSI 3080/3081) and a condensation particle counter (CPC, TSI 3775), with a time resolution of 3 min. The flow rate through the devices was 0.30 ± 0.01 l/min (NTP). The particles were size classified according to their electrical mobility by the DMA and the number of particles in each size class was counted by the CPC (with a counting efficiency higher than 96%). In the case of spherical particles, the (electrical) mobility diameter of particles is equal to the geometric diameter (Hinds, 1999). The measurement range was from 15 to 670 nm (64 size channels per decade). However, a pre-impactor removed particles larger than 615 nm at the inlet of the DMA. The measurement system was controlled with the Aerosol Instrument Manager software version 9.0 (TSI). This measurement system is called Scanning Mobility Particle Sizer (SMPS).

The number size distribution of particles was also measured online with an Electrical Low Pressure Impactor (Classic ELPI®, Dekati Ltd model 97 2E) with a time resolution of 1 s. Inside the ELPI, particles were charged with a corona charger and then differentiated by their aerodynamic diameter on twelve impaction stages inside the cascade impactor. The aerodynamic diameter is defined as the diameter of a spherical particle with a density of 1 g/cm^3 (the density of a water droplet) that has the same settling velocity as the measured particle (Hinds, 1999). The number concentration of particles on each impaction stage was derived from the electrical charge of particles and the measured electrical current from the stages. The inlet of the impactor was at ca. atmospheric pressure and the outlet was at 100 mbar (absolute). The flow rate through ELPI was 9.75 ± 0.20 l/min (NTP). The measurement range of the ELPI was from ca. 7 nm – 10 μm (less than 5 size channels per decade). The measurement uncertainty was ±10%. The measurement system was controlled with the ELPIVI software version 4.0 (Dekati Ltd).

All the presented online measurement data was corrected considering the loading of the analysis filter by particles and the consequent decrease in the flow rate through the filter and thus the decreased flow rate into the aerosol sampling line from the main line (see reference (Kajan et al., 2017b)). The correction was based on the calibration of flow rate through the critical orifice (CO) at

various temperatures and pressures simulating the loading of the filter. The calibration data was then utilized to estimate the flow rate through the CO in the experiments with the help of temperature and pressure measurement data. The flow rate from the main line to the aerosol line was also measured with the Thermal Mass Flowmeter at the beginning of every experiment. As a result, the changes in dilution ratio could be taken into consideration. The highest uncertainty in the dilution ratio originated from the inaccuracy of the mass flow controller feeding air through the porous tube dilutor and of the Thermal Mass Flowmeter. Given that the uncertainty of both devices can be ±2% of the reading, the uncertainty in the dilution ratio was ca. ±4%. Otherwise the contribution of uncertainties in temperature and pressure measurements to the dilution ratio was low, since the flow rate through the critical orifice did not vary significantly due to these uncertainties. The presented online data was also dependent on the flow rate through the main line. The flow rate was always measured in the beginning of experiments, and thus an additional uncertainty of ±2% resulted from the flowmeter. Therefore, the combined conservative uncertainty estimate for the presented online data due to gas flow rate was ca. ±6%. As a result of considering all the uncertainty sources in the online data, the highest measurement uncertainty is for the ELPI data, ca. ±16% (conservative estimate).

2.4. Analysis methods of ruthenium release and transport

The release rate of ruthenium from the crucible inside the furnace was obtained by weighing the mass of the crucible with RuO_2 powder before and after the experiment. The uncertainty in the weighing results was ca. ±2.5%. The mass of released RuO_2 was then converted to the corresponding mass of elemental ruthenium. Based on the previous study performed with the same facility using a ^{103}Ru radiotracer (Kärkelä et al., 2007), the release of ruthenium from the crucible was assumed to be linear during the experiment. The feed of CsI was analysed by weighing the supply bottle of the atomizer with CsI 4 wt % solution before and after the experiment. The uncertainty in the weighing results was ca. ±2.5%.

The quantification of gaseous ruthenium trapped in the sodium hydroxide liquid traps and ruthenium aerosols collected on filters was performed using INAA (Instrumental Neutron Activation Analysis). Ruthenium in the liquid traps was precipitated by addition of EtOH (96% Sigma-Aldrich), centrifuged and then filtered from the solution. Aerosols collected on the PTFE filters were used as they were after the experiment. Samples were then irradiated in the research reactor at VTT (Triga mark II reactor in Otaniemi, Espoo). Irradiations were performed with a thermal neutron flux of $8.7 \cdot 10^{12}$ n·cm^{-2}·s^{-1} and epithermal flux of $4.6 \cdot 10^{12}$ n·cm^{-2}·s^{-1}. Samples were irradiated from 10 min up to 4 h depending on the ruthenium content of the sample. After one week of cooling time, samples were measured by gamma spectrometry. For the measurements a High Purity Germanium (HPGe) detector (Ortec model GEM-15180-S) was used with a relative efficiency of 17.7% and resolution of 1.7 keV, both at 1332 keV. The evaluation of data was carried out with GammaVision software version 7.01.03. (Ortec). The detector was empirically calibrated for both energy and efficiency with QCYA18189 (Eckert & Ziegler) standard radionuclide source solution with the same geometry as irradiated samples. The activity of ^{103}Ru was determined from counts at the 497 keV peak, where absolute efficiency at the given geometry was determined to be 1.7%. The activity of ^{134}Cs was determined from counts at the 605 keV peak, where absolute efficiency at the given geometry was determined to be 1.5%. The compensation for the true coincidence summing was performed when necessary during evaluation of ^{134}Cs quantities in the samples. The detection limit for ruthenium and caesium was determined to be 1.0E-2 μg based on the times of irradiations and measurements. Detection of iodine on the filters was not possible by means of INAA due to the low half-life of ^{128}I ($T_{1/2}$ = 25min) and due to the evaporation of iodine during the neutron activation. The uncertainty of measurements in the experiments with the feed of CsI was calculated to be 5% according to GUM (Guide to the Expression of Uncertainties in Measurements) (Metrology, 2008). The uncertainty of measurements in the experiments with air atmosphere without additives was calculated to be ±10% due to the necessity of geometry corrections for the detector calibration.

The quantification of iodine and caesium trapped in the sodium hydroxide liquid traps was performed using Inductively Coupled Plasma Mass Spectrometry (ICP-MS). The analysis was performed after the precipitation and filtration of ruthenium in the liquid traps. A Thermo Scientific™ HR ICP-MS Element2™ Inductively Coupled Plasma Mass Spectrometer was used to measure the concentrations of minor and trace iodine and caesium in aqueous solution of sodium hydroxide 0.1 M. The mass resolution (m/Δm) of the ICP-MS was 300. The optimization of the experimental parameters was performed using the maximum ion intensity of ^{127}I, ^{133}Cs and ^{103}Rh. All solutions were prepared using sodium hydroxide solution (0.1 M). In addition, the elution buffer contained an internal standard of 10 μg/l Rh (Rhodium, element standard for atomic spectroscopy 1000 ± 5 μg/ml, 20 °C, Spectrascan). Iodine standard solutions were prepared by dissolving the appropriate amount of potassium iodide (Pro Analysis grade) in MilliQ water after dilutions with sodium hydroxide. Caesium standard solutions were prepared by diluting standard solutions obtained from SPEX CertiPrep (CLMS-2 Claritas PPT ICP-MS solution). The ICP-MS was rinsed with 1% nitric acid solution and 0.1 M sodium hydroxide solution for a total of 7 min between aliquot measurements to reduce the memory effect of iodine. After samples with an assumable high concentration of iodine, 5% nitric acid solution was used for rinsing instead of 1% nitric acid solution. No specific sample preparation was required and dilutions were performed in the same matrix. Data evaluation was performed with The Element ICP-MS Software (version 3.12.242). The uncertainty in the ICP-MS analysis was ca. ±1.0% for caesium and ca. ±0.5% for iodine.

Chemical analysis of the collected aerosol samples was carried out using XPS (X-ray photoelectron spectroscopy). With the use of XPS the elemental composition of the samples as well as the oxidation states of detected elements was determined. For the XPS measurements, a Perkin Elmer Phi 5500 Multi Technique System was used. The detailed setup of the machine during measurements was described in a previous work (Kajan, 2014). Commonly, the C 1s peak is used as an internal standard for the binding energies during XPS measurements. In the case of ruthenium, the Ru 3d5/2 peak overlaps with the C 1s peak, which makes this reference unreliable, and therefore gold foil conductively connected to the measured samples was used as an internal standard during the measurements. The experimental uncertainty of binding energy for the Ru $3d_{5/2}$ peak was determined to be ±0.1 eV. The collected spectra were curve fitted with PHI Multipak software (Ulvac-Phi inc.) assuming Shirley background. The asymmetrical shape of peaks was used due to the conductive nature of anhydrous RuO_2 (Mun et al., 2007a). XPS analysis was performed from at least two different spots on the samples.

The size and morphology of particles transported through the facility and then collected on perforated carbon-coated nickel grids were analysed with a Scanning Electron Microscope (SEM, Merlin® FEG-SEM, Carl Zeiss NTS GmbH).

2.5. Dynamic shape factor of non-spherical particles

For a spherical particle of unit density, the size can be simply

characterized by the geometric diameter. For particles of arbitrary shape and density, an equivalent diameter is used, such as electrical mobility diameter and aerodynamic diameter (Kulkarni et al., 2011). If the studied particles are non-spherical, a correction factor called the dynamic shape factor χ is needed to account for the effect of shape on particle motion. Since SMPS and ELPI devices use different operation principles, the measured mobility and aerodynamic diameters of non-spherical particles are converted to a common volume equivalent diameter d_{ve} (see the method presented in (Hinds, 1999; Signorell and Reid, 2011)). This can be thought of as the diameter of the sphere that would result if the irregular particle melted to form a droplet (Hinds, 1999). In the case of the mobility diameter, the volume equivalent diameter is as follows:

$$d_{ve} = d_m \frac{C_s(d_{ve})}{\chi C_s(d_m)}, \quad (1)$$

where $C_s(d_m)$ and $C_s(d_{ve})$ are the Cunningham slip correction factors (Hinds, 1999) for the mobility diameter and the volume equivalent diameter, respectively (DeCarlo et al., 2004). Note that for a spherical particle $\chi = 1$, the volume equivalent, mobility and geometric diameters are equal. Similarly, the volume equivalent diameter is related to the aerodynamic diameter by:

$$d_{ve} = d_a \sqrt{\chi \frac{\rho_0}{\rho_p} \frac{C_s(d_a)}{C_s(d_{ve})}}, \quad (2)$$

where ρ_0 is the reference density (1 g/cm^3), ρ_p is the density of the particle and $C_s(d_a)$ is the Cunningham slip correction factor for the aerodynamic diameter (Hinds, 1999). The relationship between mobility and aerodynamic diameter can be determined by combining Equations (1) and (2):

$$d_m = d_a \chi^{\frac{3}{2}} \sqrt{\frac{\rho_0}{\rho_p}} \frac{C_s(d_m)\sqrt{C_s(d_a)}}{C_s(d_{ve})^{\frac{3}{2}}} \quad (3)$$

Since both d_m and d_a are measured with SMPS and ELPI, and the density of particles ρ_p is known for our samples, Equation (3) can be used to empirically determine the dynamic shape factor χ.

3. Results

3.1. Release and transport results

The results of ruthenium release from the crucible and transport into the filter and trapping bottles are summarized below. The mass flow rates are presented as of ruthenium(0), not of the oxides. Similarly, the mass flow rates of caesium and iodine are given as pure elements. The results are normalised to a flow rate of 5 l/min (NTP), because the carrier gas flow rate through the main line filter and the trapping bottle was not, due to the online sampling, the same in all experiments (see Chapter 2.3). In order not to overestimate the presented uncertainties in these main analysis results, the propagation of uncertainties (originating mainly from the flow rate uncertainties) was estimated more accurately according to reference (Metrology, 2008).

3.1.1. Ruthenium release from the crucible

The release rate of ruthenium from the crucible was determined by weighing the crucible with RuO_2 powder before and after each experiment. The difference in mass was converted to the mass of elemental ruthenium and it was divided by the duration of experiment in minutes. Based on the previous study (Kärkelä et al., 2007), the release rate was assumed to be linear. The obtained results are presented in Table 2.

As can be seen from Table 2, the release rate of ruthenium was strongly dependent on the temperature in the experiments. There was a high increase in the release rate when temperature increased from 1300 K to 1700 K. The feed of CsI particles did not have a noticeable effect on the release rate of ruthenium. The results were similar at 1500 K in humid air atmosphere with and without CsI feed. A lower oxygen partial pressure due to addition of steam into the system led to a slightly lower release of ruthenium when compared to a dry air atmosphere, see experiments 4 and 6. This observation was similar to those made in the previous studies (Kärkelä et al., 2007; Kajan et al., 2017b).

3.1.2. Ruthenium transport in air atmosphere

The transport of ruthenium both in the forms of gas and aerosol in air atmosphere at different temperatures are summarized in Table 3. The ratio between aerosol and gaseous forms of ruthenium is also presented. The corresponding fractions of transported ruthenium given as % of the released ruthenium are presented in Table 4. The results are based on INAA analysis.

Based on the data presented in Tables 3 and 4, an important effect of temperature was observed on the absolute amount of transported ruthenium, as well as on its chemical form. The overall transport of ruthenium increased when temperature increased. The low amount of steam in experiment 2 did not have as prominent effect on the transport of ruthenium when compared with the effect of temperature. A notable increase in ruthenium transport was detected when the temperature increased from 1300 K to 1500 K. The transport rate of RuO_2 aerosol increased by a factor of ca. 19. Further increase in temperature to 1700 K did not lead to a similar increase in the RuO_2 transport rate, although a significant increase in the ruthenium transport through the facility was observed. From the ratio between aerosol and gaseous forms of ruthenium it can be seen that ruthenium in the form of aerosol was predominant over RuO_4 throughout the whole temperature range of the experiments (1300 K–1700 K).

On the other hand, the fraction of transported gaseous ruthenium was the lowest at 1500–1700 K. Based on the thermodynamic equilibrium calculations (Backman et al., 2005; Kajan et al., 2017a), the formation of RuO_4 should increase when temperature increases from 1300 K to 1700 K. However, at the same time the ratio between RuO_4 and RuO_3 decreases in the calculations. Most probably, the formed RuO_4 had decomposed and condensed to RuO_2 on the surface of existing RuO_2 particles in the gas flow within the model primary circuit. This phenomenon could be even stronger at high temperatures when the formation of RuO_3 (Backman et al., 2005) and thus the transport of RuO_2 particles are enhanced. The highest fraction of transported gaseous ruthenium was observed at 1300 K, when ca. 5.2% of the released ruthenium was in gaseous form at the outlet of the facility and thus it induced a partial pressure of 10^{-6} bar (calculated as RuO_4). The gaseous ruthenium transport corresponds to ca. 45% of the total transported ruthenium.

Table 2
The release rates of ruthenium from the crucible. Values are presented as mass of ruthenium metal.

Experiment	Ruthenium release rate [mg/min]
1. (1300 K)	1.0 ± 0.03
2. (1500 K)	5.6 ± 0.1
3. (1700 K)	25.4 ± 0.6
4. (CsI 1300 K)	0.66 ± 0.02
5. (CsI 1500 K)	5.6 ± 0.1
6. (CsI 1700 K)	24.8 ± 0.6

Table 3
The transport of ruthenium as RuO_2 aerosol particles and RuO_4 gas through the model primary circuit. The uncertainties are given as one standard deviation. Values are presented as mass of ruthenium metal.

Exp.	Ru in the form of RuO_2 aerosol [mg/min]	Ru in the form of RuO_4 gas [mg/min]	Ratio of RuO_2/RuO_4
1. (1300 K)	0.065 ± 0.007	0.052 ± 0.006	1.25 ± 0.08
2. (1500 K)	1.20 ± 0.13	0.012 ± 0.001	100 ± 6
3. (1700 K)	8.8 ± 0.9	0.055 ± 0.006	160 ± 10

Table 4
The fractions of ruthenium transported as RuO_2 aerosol particles and RuO_4 gas through the model primary circuit, and the fraction of ruthenium deposited inside the circuit. All values are given as % of the released Ru. The uncertainties are given as one standard deviation.

Exp.	Ru transported in total [%]	RuO_2 transported [%]	RuO_4 transported [%]	Ru deposited [%]
1. (1300 K)	11.7 ± 1.3	6.5 ± 0.7	5.2 ± 0.6	88.3 ± 1.3
2. (1500 K)	21.6 ± 2.4	21.4 ± 2.3	0.21 ± 0.02	78.4 ± 2.4
3. (1700 K)	34.9 ± 3.8	34.7 ± 3.8	0.22 ± 0.02	65.1 ± 3.8

Most of the ruthenium was deposited inside the facility (determined from the difference of the analysed release and transport of ruthenium). The fraction of deposited ruthenium decreased from 88% to 65% when temperature increased from 1300 K to 1700 K. A significant area of deposition was visually observed to be located at the outlet of the furnace, where the temperature gradient was the highest (Kärkelä et al., 2008). This is in agreement with previous observations (Kärkelä et al., 2007).

3.1.3. Ruthenium transport in humid air atmosphere with airborne CsI

The transport of ruthenium both in the forms of gas and aerosol in humid air atmosphere with airborne CsI at different temperatures is summarized in Table 5. The ratio between aerosol and gaseous forms of ruthenium is also presented. The corresponding fractions of transported ruthenium given as % of the released ruthenium are presented in Table 6. The results are based on INAA analysis.

The feed of CsI aerosol to the flow of ruthenium oxides decreased the overall transport of ruthenium through the facility at temperatures of 1300 K and 1700 K, whereas at 1500 K the ruthenium transport was on the same level as in the pure humid air atmosphere. The fraction of ruthenium transported in gaseous form was significantly increased at 1500 K and 1700 K. This effect was most prominent at 1500 K, at which about 16.4% of the released ruthenium was transported in gaseous form when compared to the fraction of 0.2% in the case of the pure humid air atmosphere. This corresponds to ca. 80% of the total transported ruthenium. The transport rate of ruthenium as gas was ca. 0.92 and 1.5 mg/min at 1500 K and 1700 K, respectively. This corresponds to a partial pressure of 10^{-5} bar (calculated as RuO_4). This is the highest amount of Ru ever observed in gaseous form in the experiments with this facility.

The transport of ruthenium in aerosol form was significantly decreased at all temperatures in contrast to the pure air atmosphere. However, the trend was similar and the aerosol transport increased with temperature. From the ratio between the aerosol and gaseous forms of ruthenium it can be seen that ruthenium in the form of a gas was predominant over RuO_2 at 1300 K and 1500 K. The aerosol transport of ruthenium was slightly greater than the gaseous transport at 1700 K.

The feed of CsI and the transport of caesium and iodine through the model primary circuit in experiments 4 to 6 and the corresponding fractions of the fed amount of both elements are summarized in Tables 7–9 (INAA analysis of particles on filter; ICP-MS analysis of gaseous compounds trapped in liquid trap). The quantification of iodine collected on the filter was not possible due to the evaporation of iodine during the neutron activation, and thus the available data is only for the iodine trapped in the liquid trap.

Based on the INAA and ICP-MS analyses, the overall transport of both caesium and iodine through the facility was less than 1% of the fed caesium and between 1 and 5% of the fed iodine. Caesium was transported mainly as aerosol particles. The observed volatile fraction of caesium was very low, whereas the ICP-MS analyses indicated that part of the iodine had separated from the fed CsI compound and iodine was transported in gaseous form to the liquid traps. Although iodine appeared to be transported significantly as a gas, some iodine was detected on the filter samples in the XPS analysis (see below). Thus, due to the evaporation of iodine in the INAA analysis, the overall quantification of the transported iodine is underestimated. The transport of both caesium and iodine in total increased with increasing temperature.

More than 79% of the released ruthenium was deposited inside the facility. In the case of caesium, the deposited fraction was very high at ca. 99%, whereas for iodine the deposition was over 95%. As in the air atmosphere, the deposition of these elements decreased when temperature increased. The deposition was determined from the difference of the analysed release and transport of the elements.

3.1.4. Online monitoring of aerosol transport

The transport of aerosol particles was monitored online in order to obtain information on the transient behaviour of ruthenium in the facility. The properties of particles, such as number concentration, diameter and number size distribution, were measured with SMPS and ELPI at the outlet of the facility. The range of

Table 5
The transport of ruthenium in the forms of aerosol and gas through the model primary circuit with additional airborne CsI aerosol. The uncertainties are given as one standard deviation. Values are presented as mass of ruthenium metal.

Exp.	Ru in the form of aerosol [mg/min]	Ru in the form of gas [mg/min]	Ratio of Ru aerosol/Ru gas forms
4. (CsI 1300 K)	0.022 ± 0.001	0.026 ± 0.002	0.85 ± 0.04
5. (CsI 1500 K)	0.24 ± 0.02	0.92 ± 0.06	0.26 ± 0.01
6. (CsI 1700 K)	2.7 ± 0.2	1.5 ± 0.1	1.8 ± 0.1

Table 6
The fractions of ruthenium transported in the forms of aerosol and gas through the model primary circuit with additional airborne CsI aerosol, and the fraction of ruthenium deposited inside the circuit. All values are given as % of the released Ru. The uncertainties are given as one standard deviation.

Exp.	Ru transported in total [%]	Ru transported in the form of aerosol [%]	Ru transported in the form of gas [%]	Ru deposited [%]
4. (CsI 1300 K)	7.3 ± 0.5	3.3 ± 0.2	3.9 ± 0.3	92.7 ± 0.5
5. (CsI 1500 K)	20.7 ± 1.4	4.3 ± 0.3	16.4 ± 1.1	79.3 ± 1.4
6. (CsI 1700 K)	16.9 ± 1.1	10.9 ± 0.7	6.0 ± 0.4	83.1 ± 1.1

Table 7
The feed of CsI and the transport of caesium in the form of aerosol and both caesium and iodine in the form of gas through the model primary circuit. The uncertainties are given as one standard deviation. Values are presented as elemental caesium and iodine.

Exp	CsI feed[a] [mg/min]	Cs in the form of aerosol [mg/min]	Cs in the form of gas [mg/min]	Iodine in the form of gas [mg/min]
4. (CsI 1300 K)	4.2 ± 0.1	8.4E-3±5.1E-4	4.2E-5±1.5E-6	3.6E-2±1.3E-3
5. (CsI 1500 K)	4.1 ± 0.1	1.4E-2±8.5E-4	3.1E-4±1.1E-5	5.5E-2±1.9E-3
6. (CsI 1700 K)	4.0 ± 0.1	1.5E-2±9.1E-4	5.4E-5±2.0E-6	9.3E-2±3.3E-3

[a] The feed of CsI was analysed by weighing the supply bottle of the atomizer before and after the experiment.

Table 8
The fractions of caesium transported in the forms of aerosol and gas through the model primary circuit, and the fraction of caesium deposited inside the circuit. All values are given as % of the fed caesium in the form of CsI. The uncertainties are given as one standard deviation.

Exp.	Cs transported in total [%]	Cs transported in the form of aerosol [%]	Cs transported in the form of gas [%]	Cs deposited [%]
4. (CsI 1300 K)	0.39 ± 0.03	0.39 ± 0.03	2.0E-3±8.6E-5	99.61 ± 0.03
5. (CsI 1500 K)	0.68 ± 0.04	0.67 ± 0.04	1.5E-2±6.5E-4	99.32 ± 0.04
6. (CsI 1700 K)	0.74 ± 0.05	0.73 ± 0.05	2.6E-3±1.2E-4	99.26 ± 0.05

Table 9
The fractions of iodine transported in the forms of aerosol and gas through the model primary circuit, and the fraction of iodine deposited inside the circuit. All values are given as % of the fed iodine in the form of CsI. The uncertainties are given as one standard deviation.

Exp.	I transported in total [%]	I transported in the form of aerosol[a] [%]	I transported in the form of gas [%]	I deposited [%]
4. (CsI 1300 K)	1.75 ± 0.08	–	1.75 ± 0.08	98.25 ± 0.08
5. (CsI 1500 K)	2.75 ± 0.12	–	2.75 ± 0.12	97.25 ± 0.12
6. (CsI 1700 K)	4.76 ± 0.20	–	4.76 ± 0.20	95.24 ± 0.20

[a] The analysis of iodine transport in the form of aerosol was not possible with INAA.

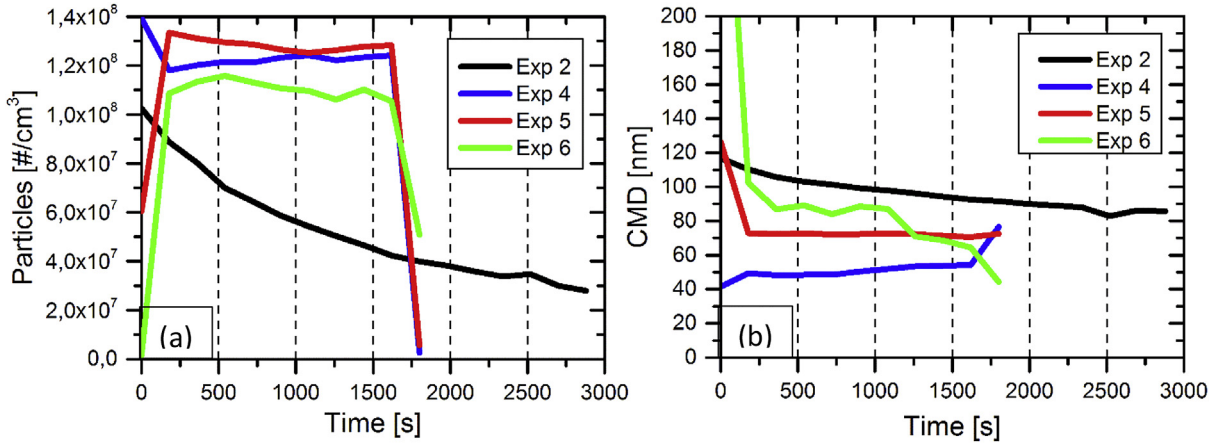

Fig. 2. The particle number concentration [#/cm^3] (a) and count median diameter [nm] (b) at the outlet of the facility during the experiments (measured with SMPS). The duration of experiment 2 was 51 min, whereas the other experiments all lasted for 30 min.

conservative estimate on the measurement uncertainty, ±10% and ±16% for the devices in the experiments, respectively, is not displayed in Figs. 2 and 3 below. The continuous online data of experiments 1 (Kärkelä et al., 2007) and 3 (Backman et al., 2005) are not available.

The evolution of particle number concentration and the count median diameter (CMD) of particles in the experiments is shown in Fig. 2 (measured with SMPS). The vaporization temperature of ruthenium inside the furnace had an effect on the diameter of particles. The CMD of particles increased from 40 nm (Kärkelä et al., 2007) to 100 nm and to 140 nm (Backman et al., 2005) when the temperature increased from 1300 K to 1500 K and to 1700 K in the air atmosphere. This observation is also supported by the previous study on the behaviour of ruthenium in air/nitrogen compounds

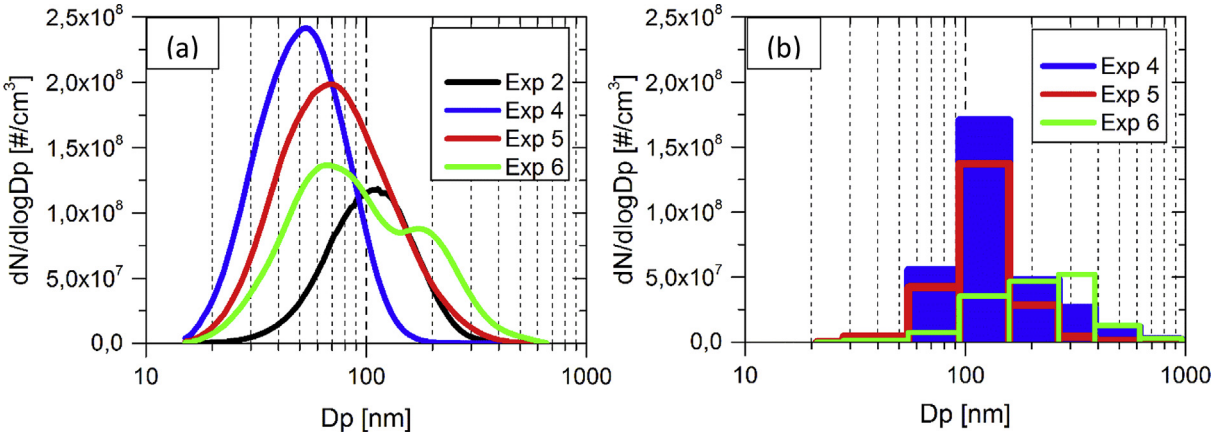

Fig. 3. The particle number size distribution 900 s after the beginning of the experiment (measured with (a) SMPS and (b) ELPI).

mixtures (Kajan et al., 2017a). This phenomenon is directly connected to a higher release of ruthenium from the crucible and to the subsequent formation of particles. High release of ruthenium also favours the agglomeration of particles, when the concentration of particles exceeds ca. 10^6 particles per cm^3 (Hinds, 1999). A similar increase in CMD from 50 to 90 nm was also observed in humid air when CsI was present in the gas flow, see Fig. 2. However, the diameter of particles appeared to be lower at 1500 K and 1700 K when compared to the reference experiments 2 and 3. Most probably this is due to the high formation of gaseous RuO_4 (see above) and therefore the nucleation of RuO_2 particles was decreased. At 1300 K the particle CMD was slightly higher when CsI was fed into the flow of Ru oxides. Overall, the transport of ruthenium as particles and gas was rather close to that in the reference experiment 1 at this temperature.

The particle number concentration was in a range from $1 \cdot 10^6$ to $1 \cdot 10^8$ particles per cm^3 in air atmosphere at all temperatures. As CsI was airborne, it resulted in an even higher concentration of particles, $1.1 \cdot 10^8$ to $1.3 \cdot 10^8$ particles per cm^3. The number concentration of particles decreased as the CMD of particles increased. This was clearly obvious at 1700 K, when the release of Ru was the highest and the formation of RuO_2 particles and their agglomerates were pronounced.

The particle number size distribution 900 s after the beginning of the experiment is presented in Fig. 3 (measured with SMPS and ELPI). The data is presented for a particle diameter range from 15 to 1000 nm. In addition to the above observations on particle behaviour, it was observed that the transported particles were lognormally distributed and most of the particles were smaller than 600 nm in diameter. The shape of the particle number size distribution did not vary much due to the feed of CsI compound in the studied conditions. The measured distributions were wider when the temperature increased. At 1700 K two modes were observed; the second mode with a higher particle diameter was probably composed of the large agglomerate particles.

The details of the measured number size distributions were more visible in SMPS data. The rather robust division of particles by diameter in ELPI data resulted in the interpretation of experiments 4 and 5 to have particles with similar size distributions. The difference between the experiments was clear in SMPS data. There was also a difference in the measured particle diameter, see Fig. 3. This difference is explained by the different measurement techniques. SMPS measured the mobility diameter of particles, whereas ELPI measured their aerodynamic diameter. This is further discussed in Sections 2.5 and 3.3.

3.2. Chemical characterization

3.2.1. XPS analysis

The transported aerosol particles were collected on PTFE filters (see “filter 2” in Fig. 1) and analysed with XPS. In the analysis the electron binding energies of the Ru 3d5/2, I 3d5/2 and Cs 3d5/2 peaks were examined. The measured binding energies were thereafter compared with reference values from the literature, and thus the chemical form of aerosols could be determined. The reference electron binding energies for the studied elements Ru, I and Cs in the experiments are presented in Table 10. The binding energies are given for various compounds. The measured XPS spectra in experiments 4 to 6 are given in the Supplementary Figs. SF3-SF11 for Ru, I and Cs.

The measured electron binding energies on the aerosol samples, as well as the identified compounds in experiments 4 to 6 with additional airborne CsI, are presented in Table 11. The XPS analyses of ruthenium-containing aerosols in the experiments in dry and humid air atmospheres were performed previously (Kajan et al., 2017b) and ruthenium was observed to be in the forms of RuO_2 and partially hydrated RuO_2.

On the basis of the measured electron binding energies in the aerosol samples of all the experiments, ruthenium was in the form of RuO_2. The binding energy of Ru 3d5/2 peak (in a range from 280.8 to 281.3 eV) was slightly higher than the reference binding energy for anhydrous RuO_2 (280.5 eV) (Kajan et al., 2016), see Table 11. Therefore it can be assumed that RuO_2 was in partially hydrated form in the experiments conducted at 1500 K and 1700 K, in which the amount of adsorbed water was lower than the stoichiometry of reference hydrated samples $RuO_2 \cdot H_2O$ (282.1 eV) (Kajan et al., 2016). At 1300 K the binding energy of Ru 3d5/2 peak was within the same region as for RuI_3 compound, see Table 10. Thus, the formation of RuI_3 aerosol cannot be ruled out in this experiment. The measured electron binding energy in all experiments was also significantly lower than for the ruthenium in its perruthenate form (binding energy ≈ 284.2 eV). This observation does not support the possibility that ruthenium is transported in the form of $CsRuO_4$ or Cs_2RuO_4, when both caesium iodide and ruthenium are present in an RCS at the same time. The transportation of ruthenium partly in form of caesium compounds was observed in the RUSET program when Cs was mixed with the metallic ruthenium precursor at ca. 1370 K (Vér et al., 2010). The formation of Cs_2RuO_4 was suggested. In a recent study (Di Lemma et al., 2015), significant formation of Cs_2RuO_4 was predicted and observed experimentally by Raman spectroscopy on collected aerosols to take place at temperatures above 1700 K and the compound was also observed when the Ru-

Table 10
The reference binding energies (eV) of Ru 3d5/2, I 3d/52 and Cs 3d5/2 for various compounds.

Compound	Ru 3d5/2	I 3d5/2	Cs 3d5/2
Ru metal	280.0 (Kim and Winograd, 1974)	–	–
RuO_2	280.5 (Kajan et al., 2016)	–	–
$RuO_2 \cdot H_2O$	282.1 (Kajan et al., 2016)	–	–
$BaRuO_4$	284.2 (Ohyoshi et al., 1980)	–	–
RuO_4	283.3 (Kim and Winograd, 1974)	–	–
$RuI_3 \cdot H_2O$	281.5[a]	619.0[a]	–
I_2	–	620.2 (Wagner et al., 1979) 619.9 (Sherwood, 1976; Dillard et al., 1984)	–
I_2O_5	–	623.3 (Sherwood, 1976)	–
HIO_3	–	623.1 (Sherwood, 1976)	–
$NaIO_4$	–	624 (Sherwood, 1976)	–
CsI	–	618.4 (Morgan et al., 1973)	724.1 (Morgan et al., 1973)
CsOH	–	–	724.15 (Wagner et al., 1979)
Cs_2O	–	–	725.2 (Yang and Bates, 1980)
$CsClO_4$	–	–	724.4 (Morgan et al., 1973)

[a] The measured reference XPS spectra are given in the Supplementary Figs. SF1-SF2 for Ru and I.

Table 11
The measured electron binding energies (eV) and identified compound/ions of the collected aerosols in experiments 4 to 6 at 1300 K–1700 K.

Peak	Exp. 4 (CsI 1300 K)			Exp. 5 (CsI 1500 K)			Exp. 6 (CsI 1700 K)		
	Ru 3d5/2	I 3d5/2	Cs 3d5/2	Ru 3d5/2	I 3d5/2	Cs 3d5/2	Ru 3d5/2	I 3d5/2	Cs 3d5/2
Binding energies[a]	281.3	618.9 624.0	724.2	281.0	618.5 623.0	724.0	280.8	618.4 620.4 622.9	724.0
Chemical state of element	RuO_2 and/or RuI_3	I^- IO_4^-	Cs^+	RuO_2	I^- IO_3^-	Cs^+	RuO_2	I^- I_2 IO_3^-	Cs^+

[a] The measurement uncertainty in electron binding energy was ±0.1 eV.

CsI sample was heated to 3500 K. Other investigators have also proposed that ruthenium could be transported in the form of Cs_2RuO_4 (Mun et al., 2007b).

Caesium was detected with electron binding energies of 724.0 eV and 724.2 eV for the Cs 3d5/2 peak. It was interpreted that caesium was in the form of CsI aerosol (724.1 eV). This is supported by the observation of iodide ion (I^-) with binding energy in a range from 618.4 to 618.9 eV for the I 3d5/2 peak. About 60% of iodine was in iodide form in every experiment. It is possible that part of caesium was in the form of CsOH (Cs 3d5/2; 724.15 eV), especially when the Cs binding energy was 724.2 eV. The assumption of the formation of CsOH would also agree with the observed iodine in the forms of elemental iodine (I_2), iodate (IO_3^-) and periodate (IO_4^-). At 1300 K 40% of iodine was in the form of periodate (I 3d5/2; 624.0 eV). At 1500 K 40% of iodine was in the form of iodate (I 3d5/2; 623.0 eV). At 1700 K only 10% of iodine was in the form of iodate (I 3d5/2; 622.9 eV) and the remaining 30% was observed to be elemental iodine (I 3d5/2; 620.4 eV).

Probably part of the iodine in caesium iodide had separated from the compound and formed the observed iodate/periodate at the same time as CsI was transported in the gas phase of the facility. The oxidation of iodine to the higher oxidation states was probably promoted by the oxidizing ruthenium oxides (RuO_3, RuO_4). Iodine oxides react readily with the water in air. This reaction is fast, especially in nanometer scale (Kärkelä et al., 2015), and the probable reaction product is iodic acid (HIO_3) (Lide, 2005). Some of the iodine oxides decompose to both HIO_3 and I_2 when in contact with water (Lide, 2005). The formation of HIO_3 already in the gas phase of the facility is probable. As the time scale between the experiment and XPS analysis was several weeks, the decomposition of residual iodine oxides and the consequent formation of HIO_3 and I_2 on the samples are expected, even though the samples were stored in a refrigerator before the XPS analysis. Furthermore, the periodate ion is suggested to originate from periodic acid (HIO_4), which is formed as a product of iodine oxides in contact with water.

On the basis of the INAA analysis (see above), the transport of gaseous ruthenium increased significantly in these experiments with CsI additive. It is probable that the formed iodine oxide compounds, especially HIO_3, were also oxidizing the lower oxides of ruthenium, such as gaseous RuO_2 and RuO_3, to gaseous RuO_4. Another possible explanation for the increased gaseous ruthenium transport is the formation of volatile ruthenium oxyiodides, when CsI is reacting with gaseous ruthenium oxides in the gas phase. The formation of noble metal oxohalides was studied previously by Eichler et al. (2000) and a high volatility of the formed $MOCl_3$ (M = Tc, Re) type compounds was observed. The notable transport of gaseous iodine based on the ICP-MS analysis would support this suggestion. All the analyses of aerosol samples showed a low transport of ruthenium aerosol (RuO_2) through the facility. It indicates that the main source of particles, gaseous RuO_3, was mostly consumed in other chemical reactions.

3.2.2. SEM analysis

The ruthenium particle samples were collected on perforated carbon-coated nickel grids and analysed with a scanning electron microscope (SEM). The SEM micrographs of the collected particles are presented in Fig. 4. Depending on the reaction conditions, the morphology (particle size and shape) of ruthenium (i.e. ruthenium oxide) particles varied amongst the samples. In all experiments the formation of agglomerates in the gas phase, before particles were collected on the grid, was obvious. In experiments 1 to 3, the typical crystalline needle-shaped form of RuO_2 was clearly evident and it was the dominating form of ruthenium in the samples. Thus, this observation was similar to the previous findings (Backman et al., 2005; Kärkelä et al., 2007).

The feed of CsI droplets into the flow of ruthenium oxides in

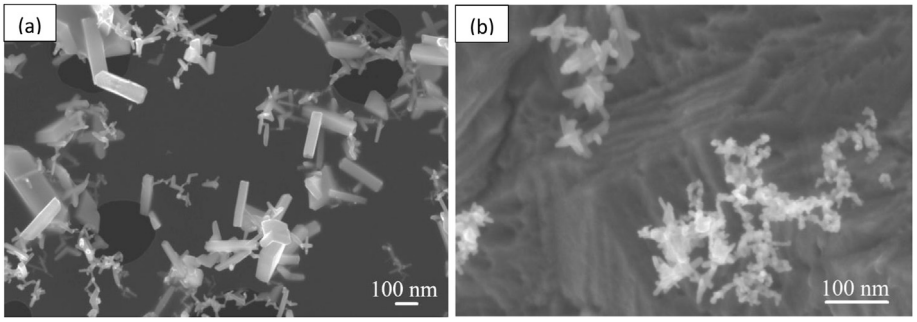

Fig. 4. SEM micrographs of ruthenium particles on a nickel/carbon grid in experiments 2 (a) and 5 (b).

Table 12
The input values and results of dynamic shape factor calculations.

Exp.	Input for calculation				Results		
	SMPS	ELPI	SMPS	ELPI	Shape factor χ	$C_s(d_{ve})$	d_{ve} [nm]
	d_m = CMD [nm]	d_a = CMD [nm]	$C_s(d_m)$	$C_s(d_a)$			
4. (CsI 1300 K)	50.3	117.0	5.09	2.62	1.32	4.94	37.0
5. (CsI 1500 K)	72.4	135.3	3.76	2.37	1.62	4.15	49.3
6. (CsI 1700 K)	87.0	206.7	3.25	1.85	1.52	3.82	67.1

experiments 4 to 6 appeared to have an effect on the shape of ruthenium particles. The needle-shaped RuO_2 crystals were still observed, but they seemed now to be in more hydrated form. This was probably due to water in the gas flow. In addition, the particle agglomerates were partly formed of very small-diameter particles. The primary particle size was dozens of nanometres, and the particles were a variety of different sized cubical crystals. The small diameter of particles was also probably due to the decreased formation of RuO_2. As presented above, the formation of gaseous ruthenium was enhanced and thus the transport of ruthenium as an aerosol was moderate.

3.3. Determination of the dynamic shape factor of particles

The dynamic shape factor of particles in experiments 4 to 6 was determined on the basis of the measured mobility and aerodynamic diameters of particles by SMPS and ELPI. The density of particles was assumed to be 6.97 g/cm^3, corresponding to solid RuO_2. For the calculation, the experimental conditions at the location of online sampling devices were assumed to be 293 K and 101 kPa. The CMD values of number size distributions presented in Fig. 3 (900 s after the beginning of experiment) were used to represent the particles in the gas flow. The input values of calculations and the results are presented in Table 12.

The obtained dynamic shape factors ranged from 1.32 to 1.62. These values correspond to a cylindrical shape, with an axial ratio between 5 and 10, and similarly to a straight chain of particles, such as agglomerates (Hinds, 1999). This is supported by the observed needle-like shape of RuO_2 particles in the SEM analysis (see above).

4. Conclusions

The effect of the airborne fission product compound CsI on the transport of ruthenium in primary circuit conditions simulating an air ingress accident is described in this paper. The gas phase reactions between ruthenium oxides and CsI were studied at 1300 K, 1500 K and 1700 K. The transport of ruthenium as gaseous and aerosol compounds through the model primary circuit, in which temperature decreased to ca. 300 K, was of interest.

The release rate of ruthenium from the evaporation crucible increased with temperature. The feed of CsI particles did not have a noticeable effect on the release rate when compared to air atmosphere with or without a low content of steam (ca. 2.1E4 ppmV). At all studied conditions, most of the released ruthenium was deposited inside the facility. Less than 35% of ruthenium was transported though the circuit. The highest transport of ruthenium was observed in air atmosphere at 1700 K. Most of the transported ruthenium was in aerosol form. However, approx. 5% of ruthenium was transported in gaseous form at 1300 K. The feed of CsI into the flow of ruthenium oxides had a significant effect on the thermodynamic equilibrium of Ru species. The transport of gaseous ruthenium increased from 0.2% up to 16% and 6% at 1500 K and 1700 K, respectively, whereas the aerosol transport of ruthenium decreased significantly. Thus the gaseous ruthenium transport corresponds to a partial pressure of 10^{-5} bar (calculated as RuO_4). This is the highest amount of Ru ever observed in gaseous form in the experiments with this facility. At 1300 K the transport of ruthenium was rather similar to that in an air atmosphere and the partial pressure of gaseous ruthenium was 10^{-6} bar, as it has been reported previously.

Based on the SEM analysis, the diameter of particles in the gas phase appeared to decrease when CsI was present. This was also supported by the online measurements of particles with SMPS. In the XPS analysis it was observed that the transported particles were mainly of partially hydrated RuO_2. Most of the iodine was still in the form of CsI on the particle samples. However, it appeared that part of the iodine had separated from CsI and oxidized to iodine oxide compounds. The process of iodine oxidation was not verified, but probably it was due to the oxidation of iodine by RuO_3 and RuO_4. The transport of gaseous ruthenium increased when CsI was airborne. The formed iodine oxide compounds could oxidize the lower oxides of ruthenium (gaseous RuO_2 and RuO_3) to gaseous RuO_4. Another possible explanation for the observed gaseous Ru transport is the formation of volatile ruthenium oxyiodides, when CsI is reacting with gaseous ruthenium oxides in the gas phase. The formation of iodic acid and periodic acid on the particle samples was probably due to contact of iodine oxides with water in the gas flow. This is also supported by the observed elemental iodine,

which is a by-product of that reaction.

It was shown in this study that airborne CsI can affect the speciation and transport of ruthenium in primary circuit conditions. The results indicated a possible increase in the fraction of gaseous ruthenium reaching the containment building during a severe nuclear accident in the case of air ingress into the reactor. The obtained new information will contribute to the knowledge on ruthenium chemistry and to the modeling of ruthenium behaviour in accident conditions, as well as to nuclear safety.

Acknowledgements

This study was performed as part of the Nordic collaboration ATR-2 (Impact of Aerosols on the Transport of Ruthenium) experimental programme, between Finland and Sweden. The financial support of SAFIR 2018, APRI 9 and NKS-R programmes is acknowledged.

Appendix A. Supplementary data

Supplementary data related to this article can be found at http://dx.doi.org/10.1016/j.pnucene.2017.04.019.

References

Backman, U., Lipponen, M., Auvinen, A., Tapper, U., Zilliacus, R., Jokiniemi, J.K., 2005. On the transport and speciation of ruthenium in high temperature oxidising conditions. Radiochim. Acta 93 (5), 297–304.

Clément, B., Cantrel, L., Ducros, G., Funke, F., Herranz, L., Rydlzv, A., Weber, G., Wren, C., 2007. State of the Art Report on Iodine Chemistry. NEA/CSNI/R, p. 1.

DeCarlo, P., Slowik, J., Worsnop, D., Davidovits, P., Jimenez, J., 2004. Particle morphology and density characterization By combined mobility and aerodynamic diameter measurements. Part 1 Theory. Aerosol Sci. Technol. 38, 1185–1205.

Di Lemma, F., Colle, J., Bene, O., Konings, R., 2015. A separate effect study of the influence of metallic fission products on CsI radioactive release from nuclear fuel. J. Nucl. Mater. 465, 499–508.

Dillard, J., Moers, H., Klewe-Nebenius, H., Kirch, G., Pfennig, G., Ache, H., 1984. X-ray and electron induced Auger processes for I2 adsorption on uranium. Spectrochim. Acta Part B At. Spectrosc. 39, 1533–1536.

Eichler, R., Eichler, B., Gäggeler, H.W., Jost, D.T., Piguet, D., Türler, A., 2000. Gas phase chemistry of technetium and rhenium oxychlorides. Radiochim. Acta 88, 87–93.

Grégoire, A.C., Haste, T., 2013. Material release from the bundle in Phébus FP. Ann. Nucl. Energy 61, 63–74.

Haste, T., Payot, F., Bottomley, P.D.W., 2013. Transport and deposition in the Phébus FP circuit. Ann. Nucl. Energy 61 (0), 102–121.

Hinds, W.C., 1999. Aerosol Technology: Properties, Behavior, and Measurement of Airborne Particles, vol. 2. Wiley, New York.

Kajan, I., 2014. RuO_4 Interaction with Surfaces in the Containment of Nuclear Power Plant, in Nuclear Chemistry. Chalmers University of Technology. ISSN 1652–943X.

Kajan, I., Lasseson, H., Persson, I., Ekberg, C., 2016. Interaction of ruthenium tetroxide with surfaces of nuclear reactor containment building. J. Nucl. Sci. Technol. 53 (9), 1397–1408.

Kajan, I., Kärkelä, T., Auvinen, A., Ekberg, C., 2017a. Effect of nitrogen compounds on transport of ruthenium through the RCS. J. Radioanal. Nucl. Chem. http://dx.doi.org/10.1007/s10967-017-5172-7. Published online: 11 January, 2017.

Kajan, I., Kärkelä, T., Tapper, U., Johansson, L.-S., Gouëllo, M., Ramebäck, H., Holmgren, S., Auvinen, A., Ekberg, C., 2017b. Impact of Ag and NOx compounds on the transport of ruthenium in the primary circuit of nuclear power plant in a severe accident. Ann. Nucl. Energy 100, 9–19.

Kärkelä, T., Backman, U., Auvinen, A., Zilliacus, R., Lipponen, M., Kekki, T., Tapper, U., Jokiniemi, J., 2007. Experiments on the Behaviour of Ruthenium in Air Ingress Accidents - Final Report. VTT research report VTT-R-01252-07.

Kärkelä, T., Pyykönen, J., Auvinen, A., Jokiniemi, J., 2008. Analysis of Flow Fields, Temperatures and Ruthenium Transport in the Test Facility. VTT research report VTT-R-00947-08.

Kärkelä, T., Vér, N., Haste, T., Davidovich, N., Pyykönen, J., Cantrel, L., 2014. Transport of ruthenium in primary circuit conditions during a severe NPP accident. Ann. Nucl. Energy 74 (0), 173–183.

Kärkelä, T., Auvinen, A., Kekki, T., Kotiluoto, P., Lyyränen, J., Jokiniemi, J., 2015. Radiolytical oxidation of gaseous iodine by beta radiation. Radiochim. Acta 103 (10), 719–728.

Kim, K., Winograd, N., 1974. X-Ray photoelectron spectroscopic studies of ruthenium-oxygen surfaces. J. Catal. 35, 66–72.

Kulkarni, P., Baron, P.A., Willeke, K., 2011. Aerosol Measurement: Principles, Techniques, and Applications, 3rd ed. John Wiley & Sons, Inc, New York.

Lide, D., 2005. CRC Handbook of Chemistry and Physics, 86th ed. CRC Press, Boca Raton (FL).

Metrology, B.J.C.f.G.i., 2008. JCGM 100:2008, Evaluation of Measurement Data – Guide to the Expression of Uncertainty in Measurement JCGM 100:2008 (GUM 1995 with Minor Corrections). Paris.

Morgan, W., Van Wazer, J., Stec, W., 1973. Inner-orbital photoelectron spectroscopy of the alkali metal halides, perchlorates, phosphates, and pyrophosphates. J. Am. Chem. Soc. 95, 751–755.

Mun, C., Ehrhardt, J., Lambert, J., Madic, C., 2007a. XPS investigations of ruthenium deposited onto representative inner surfaces of nuclear reactor containment buildings. Appl. Surf. Sci. 253 (18), 7613–7621.

Mun, C., Cantrel, L., Madic, C., 2007b. A Literature Review on Ruthenium Behaviour in Nuclear Power Plant Severe Accidents. HAL Id: irsn-00177621. https://hal-irsn.archives-ouvertes.fr/irsn-00177621.

Ohyoshi, A., Götzfried, F., Beck, W., 1980. Polynuclear carbonyl complexes of ruthenium and osmium with methylthiolate and bromine bridging ligands. Chem. Lett. 9, 1537–1540.

Sherwood, P., 1976. X-ray photoelectron spectroscopic studies of some iodine compounds. J. Chem. Soc. Faraday Trans. 2 (72), 1805–1820.

Signorell, R., Reid, J.P., 2011. Fundamentals and Applications in Aerosol Spectroscopy. CRC Press, Taylor and Francis Group, LLC.

Vér, N., Matus, L., Kunstár, M., Osán, J., Hózer, Z., Pintér, A., 2010. Influence of fission products on ruthenium oxidation and transport in air ingress nuclear accidents. J. Nucl. Mater 396, 208–217.

Vér, N., Matus, L., Pintér, A., Osán, J., Hózer, Z., 2012. Effects of different surfaces on the transport and deposition of ruthenium oxides in high temperature air. J. Nucl. Mater. 420 (1–3), 297–306.

Wagner, C., Riggs, W., Davis, L., Moudler, J., Muilenberg, G., 1979. Handbook of X-ray Photoelectron Spectroscopy. Perkin Elmer.

Yang, S., Bates, C., 1980. The role of cesium suboxides in low-work-function surface layers studied by x-ray photoelectron spectroscopy: Ag-O-Cs. Appl. Phys. Lett. 36, 675–677.